

Gleissberg Cycle Dependence of Inner Zone Proton Flux

Emily J Bregou¹, Mary K. Hudson², Brian T. Kress³, Murong Qin⁴, and Richard S. Selesnick⁵

¹University of Pennsylvania

²Dartmouth College

³NOAA - National Centers for Environmental Information (NCEI)

⁴Boston University

⁵Air Force Research Laboratory

November 21, 2022

Abstract

Inner zone proton flux from 1980 to mid-2021 is examined using NOAA POES satellite data, indicating a long-term increase corresponding to a one hundred year minimum in solar activity consistent with the Centennial Gleissberg Cycle. Variation of inner belt protons is correlated with decreasing F10.7 maxima over the 40-year period, serving as proxy for solar EUV input to Earth's atmosphere. Extending an earlier study (Qin et al., 2014) of > 70 MeV protons from 1980 – 2021 using the South Atlantic Anomaly (SAA) peak flux, and at fixed $L = 1.3$, a comparison is made between the > 35 , > 70 and > 140 MeV energy channels on POES. All three energies show an increase in proton flux over the period 1998 – 2021 using a single spacecraft. The observed flux increase is correlated with decreasing F10.7 over the longer 40-year time interval, as with the ~ 11 -year solar cycle. A phase lag during Solar Cycle 24 (January 2010 – June 2021) between the F10.7 minimum and proton flux maximum was determined to be ~ 500 days, the same at all energies studied. A model calculation of the inner zone proton flux is found to generally confirm the long-term trend examined both in absolute magnitude and phase lag. It is concluded that this long-term trend is a manifestation of the concurrent Gleissberg cycle minimum and accompanying decrease in solar EUV. Reduced EUV at solar maximum (F10.7 proxy) reduces proton loss to the atmosphere following solar maximum, thus explaining the long-term flux increase observed.

1 **Gleissberg Cycle Dependence of Inner Zone Proton Flux**

2
3 Emily J. Bregou^{1,2}, Mary K. Hudson^{1,3}, Brian T. Kress⁴, Murong Qin⁵, and Richard S.
4 Selesnick⁶

5
6 ¹ NCAR High Altitude Observatory, Boulder, CO, USA

7 ² Dept. of Physics and Astronomy, University of Pennsylvania, Philadelphia, PA, USA

8 ³ Physics and Astronomy Dept., Dartmouth College, Hanover, NH, USA

9 ⁴ Center for Cooperative Research in the Environmental Sciences at CU Boulder, Boulder, CO,
10 USA

11 ⁵ Center for Space Physics, Boston University, Boston, MA, USA

12 ⁶ Space Vehicles Directorate, Air Force Research Laboratory, Kirtland AFB, NM, USA

13
14 Corresponding author: Emily Bregou (ebregou@sas.upenn.edu)

15 **Key Points:**

- 16 • **POES MeV proton measurements from 1980-2021 are anticorrelated with**
17 **F10.7**
- 18 • **Observations are consistent with model prediction of a long term proton flux**
19 **increase**
- 20 • **Centennial Gleissberg Cycle solar minimum impact on inner zone proton**
21 **flux is found.**

22 **Plain Language Summary**

23
24 The inner zone proton radiation belt consisting of 10's to >100 MeV protons trapped in the
25 Earth's magnetic field is examined from 1980 to mid-2021 using measurements from four
26 NOAA POES satellites. A long-term increase in measured proton flux over four ~11 year cycles
27 of solar activity is found. This increase correlates with the current one hundred year minimum in
28 solar activity known as the Gleissberg cycle. Inner zone proton flux is correlated with decreasing
29 solar irradiance maxima at a wavelength of 10.7 cm, serving as proxy for Extreme Ultra Violet
30 input to Earth's atmosphere. It is found that current peak proton flux, occurring at a longitude
31 and latitude where the Earth's magnetic field is weaker, is at the highest levels seen since 1980.
32 A model calculation of the inner zone proton flux is found to generally confirm the long-term
33 trend. We conclude that this trend observed over ~ 40 years accompanies an average decrease in
34 solar EUV. The reduced EUV at solar maximum reduces proton loss to the atmosphere, thus
35 explaining the observed long-term increase in inner zone proton flux.

36 **Abstract**

37 Inner zone proton flux from 1980 to mid-2021 is examined using NOAA POES satellite data,
38 indicating a long-term increase corresponding to a one hundred year minimum in solar activity

39 consistent with the Centennial Gleissberg Cycle. Variation of inner belt protons is correlated
40 with decreasing F10.7 maxima over the 40-year period, serving as proxy for solar EUV input to
41 Earth's atmosphere. Extending an earlier study (Qin et al., 2014) of > 70 MeV protons from
42 1980 – 2021 using the South Atlantic Anomaly (SAA) peak flux, and at fixed L = 1.3, a
43 comparison is made between the > 35, > 70 and > 140 MeV energy channels on POES. All three
44 energies show an increase in proton flux over the period 1998 – 2021 using a single spacecraft.
45 The observed flux increase is correlated with decreasing F10.7 over the longer 40-year time
46 interval, as with the ~11-year solar cycle. A phase lag during Solar Cycle 24 (January 2010 –
47 June 2021) between the F10.7 minimum and proton flux maximum was determined to be ~500
48 days, the same at all energies studied. A model calculation of the inner zone proton flux is found
49 to generally confirm the long-term trend examined both in absolute magnitude and phase lag. It
50 is concluded that this long-term trend is a manifestation of the concurrent Gleissberg cycle
51 minimum and accompanying decrease in solar EUV. Reduced EUV at solar maximum
52 (F10.7proxy) reduces proton loss to the atmosphere following solar maximum, thus explaining
53 the long-term flux increase observed.

54 **1 Introduction**

55 The Earth's inner radiation belt, the first discovery of the Space Age (Van Allen et al., 1958),
56 consists of high energy protons (10 MeV–1 GeV) and lower energy electrons trapped in the
57 Earth's magnetic field. The sources of inner belt protons, the focus of this paper, include Cosmic
58 Ray Albedo Neutron Decay (CRAND) and Solar Energetic Protons (Selesnick, Hudson, &
59 Kress, 2010; Selesnick, Looper, & Mewaldt, 2007). The very energetic proton population, while
60 constrained to an altitude below $\sim 10^4$ km, is a known hazard to low and medium altitude
61 satellites (Stassinopoulos and Raymond, 1988; Dyer, 2002) and to the International Space
62 Station whose orbit encounters the South Atlantic Anomaly. The South Atlantic Anomaly (SAA)
63 is a region where the inner zone proton flux is observed to increase at low altitude. This is due to
64 a weakening in the Earth's magnetic field presently spanning a range at 500 km altitude of -90
65 to +40 degrees in geographic longitude and -50 to 0 degrees in geographic latitude. This region
66 of weaker magnetic field, which is slowly decreasing in time (Pavón-Carrasco & De Santis,
67 2016), allows inner zone protons to mirror closer to Earth.

68
69 The proton flux in the inner zone is anticorrelated with solar activity (Nakagano and Heckman,
70 1968; Dragt, 1971; Huston et al., 1998; Kuznetsov et al., 2010; Qin et al., 2014; Li et al., 2020;
71 Lin et al., 2020). During solar maximum, the upper atmosphere is heated and expands due to
72 increased solar EUV (Gombosi, 1998), so protons encounter higher neutral density along their
73 trajectories. In addition, photoionization and increased auroral activity increase ionospheric
74 density (Gombosi, 1998). The inner zone protons lose energy primarily via Coulomb collisions
75 with both free and bound electrons (Selesnick et al., 2007; Selesnick and Albert, 2019), thus
76 explaining the lower flux levels observed above a fixed energy following solar maximum. There
77 is a lag between solar maximum and proton flux minimum due to the time scale for proton
78 energy loss (Qin et al., 2014; Li et al. 2020, Lin et al., 2020). This effect on inner zone proton
79 loss dominates the solar cycle modulation of Galactic Cosmic Rays which provides the CRAND
80 source of inner zone protons and is also anticorrelated with the solar cycle (Li et al., 2020).

81
82 Previous studies have examined the solar cycle variation using different energy channels of the
83 SEM-1 and SEM-2 instruments (Rabin et al., 1995; Evans and Greer, 2006) on the NOAA Polar

84 Operational Environment Satellites (POES) in sun synchronous polar orbits at approximately
85 850 km, also used for this study. Qin et al. (2014) examined solar cycle modulation of the > 70
86 MeV proton flux from POES measurements for the period from 1980 through 2009. Li et al.
87 (2020) examined the > 36 MeV and > 140 MeV proton flux measured by a single POES
88 (NOAA-18) satellite over the shorter time interval from 2005 – 2018, also examining the
89 SAMPEX PET differential proton flux measurements (Cook et al., 1993) at 27.4 – 37.4 MeV
90 over the period 1992 – 2009. The polar orbiting (82 degree inclination) SAMPEX measurements
91 were made at an altitude of approximately 500 km (± 20 km) and $L = 1.33\text{--}1.42$. Li et al. (2020)
92 found a solar cycle modulation in the SAMPEX PET measurements at 500 km altitude of 300%
93 while at the higher altitude of POES measurements they found a solar cycle modulation of 21%.
94 Lin et al. (2020) recalibrated data from the >16-MeV proton integral fluxes obtained from
95 NOAA POES and EUMETSAT MetOp satellites, also carrying the SEM-2 instrument, from the
96 period 1978 to 2014, examining solar cycle phase lags and the relationship between trapped
97 proton fluxes and F10.7. They focused on measurements at $L = 1.2$, below the energy-dependent
98 inner zone flux peak (Ginet et al., 2013), and found no long term increase in flux at this L value
99 for > 16 MeV protons.

100

101 This paper examines data spanning a period from 1980 to the present day to illustrate a long-term
102 trend of increasing proton flux in the inner zone from the POES data set that corresponds to a
103 one hundred year minimum in solar activity. Prior studies can now be extended beyond the most
104 recent solar minimum 2018-2019, capturing the trapped proton flux increase to the highest levels
105 seen since 1980. This longer term data set allows us to investigate the Gleissberg cycle variation
106 of inner belt protons (Gleissberg, 1965). First, the study by Qin et al. (2014) of > 70 MeV proton
107 flux from 1980 through 2009 is extended through June 2021, using their method for determining
108 peak flux in the SAA, then comparing with > 70 MeV flux at fixed $L = 1.3$. A comparison is then
109 made between the > 35, > 70 and > 140 MeV energy channels on POES. The phase lag during
110 Solar Cycle 24 (January 2010 – June 2021) between F10.7 and proton flux for these three energy
111 channels is then determined. A model calculation of the inner zone proton flux based on
112 Selesnick et al. (2007) is then presented which confirms the long term trend examined here.
113 Finally, discussion and conclusions are presented in the context of the Centennial Gleissberg
114 Cycle minimum in solar activity (Gleissberg, 1965; Feynmann and Ruzmaikin, 2011; Pulkinen
115 et al., 2001) and its effect on the long term trend seen in inner zone proton flux.

116

117 **2 POES Data**

118

119 The data in this study come from the POES satellites which are low altitude polar orbiting
120 satellites launched by NOAA since 1978. The POES proton data were accessed for four
121 consecutive POES satellites: NOAA-06 (January 1st, 1980 - August 18th, 1986), NOAA-10
122 (October 11th, 1986 - January 27th 1991), NOAA-12 (January 1st 1992 - March 1st 2002), and
123 NOAA-15 (January 1st 1999 - present day). Proton counts come from an instrument on board
124 called the Space Environment Monitor or SEM with the original SEM-1 instrument aboard the
125 NOAA-06, NOAA-10, and NOAA-12 satellites and the upgraded SEM-2 aboard NOAA-15
126 (<https://www.ngdc.noaa.gov/stp/satellite/poes/>). The Space Environmental Monitors host a
127 variety of detectors to measure energetic electrons and ions (Evans and Greer, 2006).
128 Omnidirectional proton counts per second used in this application come from the medium energy
129 proton and electron detector or MEPED. This consists of a solid state detector located under a

130 hemisphere of tungsten, the thickness of which sets energy detection thresholds. To convert
 131 counts per second to omnidirectional integral flux, we calculated a conversion factor of 2.9 cm^{-2} .
 132 We used the detector front and back area of 0.5 cm^2 and side area of 0.752 cm^2 (Evans and
 133 Greer, 2006) and assumed that the detector axis was aligned with the magnetic field. In the
 134 absence of pitch angle information from the POES satellite, we assumed an isotropic proton flux
 135 outside the drift loss cone and zero flux inside. We expect the actual flux to peak at 90 degrees
 136 (Selesnick et al., 2014) which, if accounted for, would result in slightly higher measured flux.

137

138 Solar proton events or SPEs occur when particles emitted from the sun are accelerated, either in
 139 solar flares or by interplanetary shocks produced by Coronal Mass Ejections (CMEs). Proton
 140 flux is seen to increase suddenly during SPE events produced by solar flares and more gradually
 141 from CME shocks (Reames et al., 1999). Since this study focuses on long term trends, changes
 142 in the proton population that occur over shorter timescales must be removed. Protons with
 143 energies in the 10s of MeV are known to be present at high latitudes (high L-values) during SPEs
 144 but not during solar quiet times. As such, all data corresponding to time periods in which there is
 145 a high flux of 16 MeV protons at high latitude have been removed from the dataset (Qin et al.,
 146 2014).

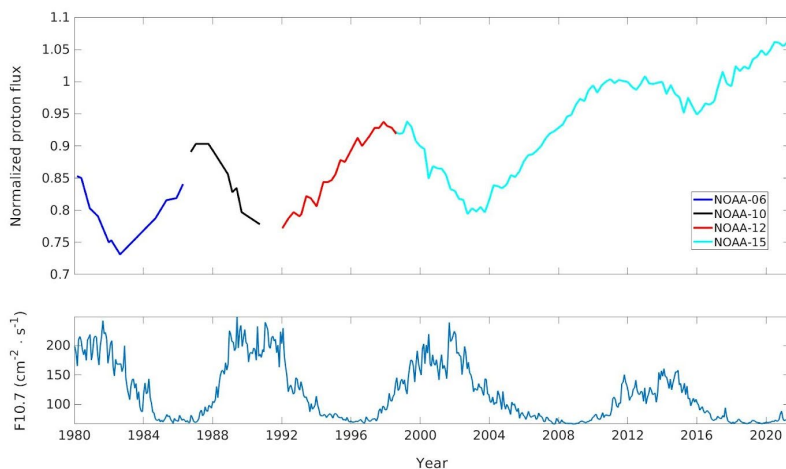
147

148 3 Observational Results

149

150 **Figure 1** is a plot of the peak flux of $>70 \text{ MeV}$ protons in the SAA from 1980 to 2021.
 151 Following the technique employed by Qin et al. (2014), we divided data into bins of 3 months.
 152 We then selected a longitudinal range of 6° corresponding to the highest flux in the SAA. A
 153 different longitudinal range was used for each of the four POES spacecraft to account for the
 154 slowly changing position of the SAA. We then fit a Gaussian in latitude to estimate the value of
 155 the peak flux. The data are normalized to one at the beginning of 2010 to facilitate comparison to
 156 Figure 3 appearing in Qin et al. (2014). F10.7 cm flux, representing solar activity, is included for
 157 comparison.

158



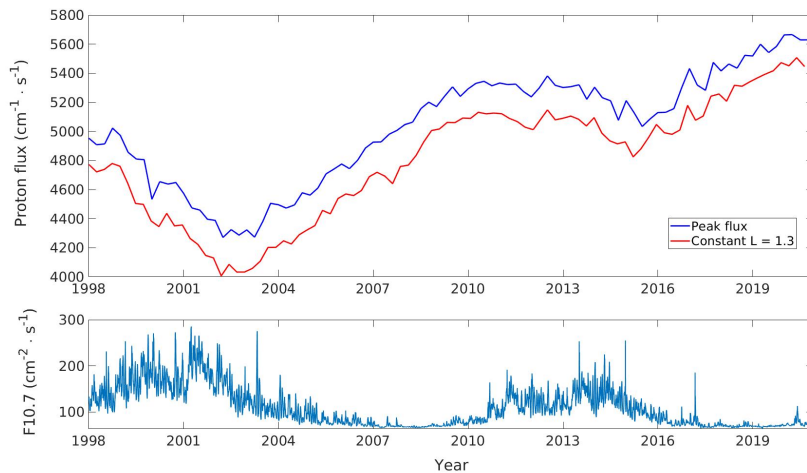
159

160 **Figure 1.** 3-month averaged peak flux for $>70 \text{ MeV}$ protons in the SAA is normalized to flux (=
 161 1) at the beginning of 2010 (top) and plotted against 10.7cm solar flux (F10.7, bottom) from
 162 1980 to June, 2021 to extend Figure 3 in Qin et al. (2014) which covered 1980 through 2009.
 163 Different colors are used to represent different POES satellites. Prior to the NOAA-15 data

164 beginning in 1999, satellites measured >80 MeV proton flux. Qin et al. (2014) found good
 165 agreement between the >80 MeV and >70 MeV proton flux data and determined that no
 166 correction factor was necessary.

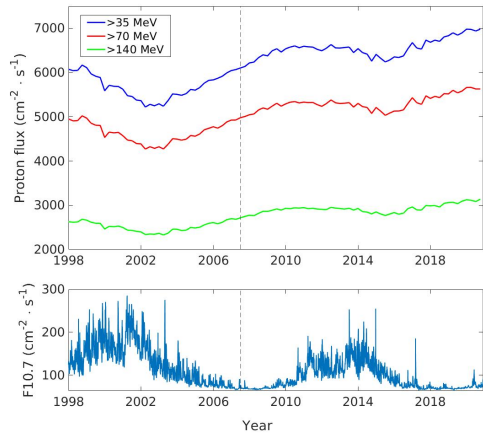
167
 168 The proton flux increases over this more than forty year time span by a factor of 1.2. It is also
 169 evident in **Figure 1** that the intensity of solar maxima as measured by F10.7 weakens over time.
 170 Superimposed on the long term trend is the solar cycle variation of both proton flux and F10.7,
 171 with a phase lag in the peak proton flux following solar minimum reported previously (Qin et al.,
 172 2014; Li et al., 2020; Lin et al., 2020) and examined further below. The magnitude of the F10.7
 173 variation is greater than the solar cycle variation of galactic cosmic rays ($>GeV$) with peak flux
 174 at solar minimum, providing a source for these trapped protons through the CRAND process
 175 (Singer et al., 1958; Li et al., 2020). This leads to the conclusion that change in atmospheric and
 176 ionospheric density with the solar cycle variation in EUV flux affects proton energy loss
 177 (Selesnick et al., 2007) and is ultimately responsible for both the solar cycle variation (Qin et al.,
 178 2014; Li et al., 2020; Lin et al., 2020) and long term trend reported here.

179
 180 In **Figure 1**, we plot the maximum flux in the SAA for >70 MeV protons found using a Gaussian
 181 (independent of L-value) fit to the maximum flux. In **Figure 2**, we plot a comparison
 182 between >70 MeV proton flux at constant $L = 1.3$ in the SAA and the maximum flux from 1998
 183 to 2021. The same trends are observed for both methodologies.
 184



185
 186
 187 **Figure 2.** (Top) >70 MeV flux at constant $L = 1.3$ in the SAA (blue) from January, 1998 to June,
 188 2021 compared with peak flux (red) from Figure 1; (Bottom) F10.7.

189
 190 **Figure 3** demonstrates that the flux increase is visible across multiple energy channels. The
 191 Solar Cycle 24 flux minimum was found to be 19% higher (averaged over energy channels) than
 192 the Solar Cycle 23 minimum. The peak flux plotted here for >35 MeV and >140 MeV protons
 193 was determined using the same Gaussian method as was used for >70 MeV protons in **Figures 1**
 194 and **2**.



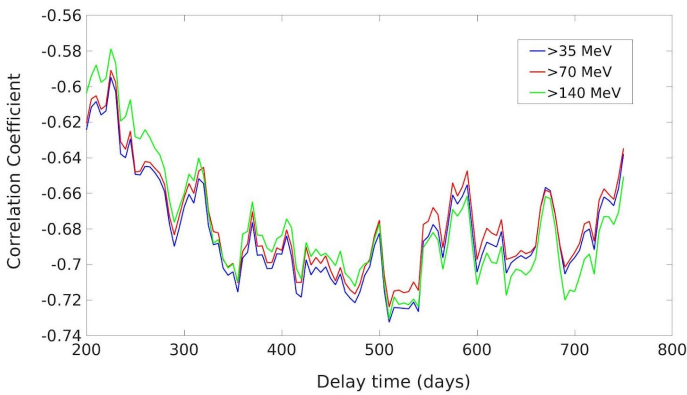
195
196

Figure 3. (Top) 3-month averaged peak flux in the SAA for >35, >70, and >140 MeV protons. A dashed line is added to indicate the change from Solar Cycle 23 to Solar Cycle 24 in 2008; (Bottom) F10.7.

199
200

We also calculated the phase lag between F10.7 and proton flux for Solar Cycle 24 for the same three energy channels that are shown in **Figure 3**. **Figure 4** shows the correlation coefficient for different phase lag values. We obtain the best fit at 510 days for all three energy channels with a correlation coefficient of 0.73. Qin et al., (2014) previously calculated the phase lag to be 705 days, 380 days, and 685 days for Solar Cycles 21, 22, and 23 respectively and did not find any dependence on proton energy. Li et al., (2020) estimated proton flux from POES satellites and sunspot number using a sine function with 11-year period and estimated a phase lag of 730 days for 2005-2015. They calculated phase lag for >36 MeV and >140 MeV protons, however, the energy dependence for phase lag was not analyzed.

201
202
203
204
205
206
207
208
209
210



211
212

Figure 4. Anticorrelation between peak proton flux in the SAA and F10.7 flux is plotted as a function of time lag for three energy channels for Solar Cycle 24 (January, 2010 - June, 2021).

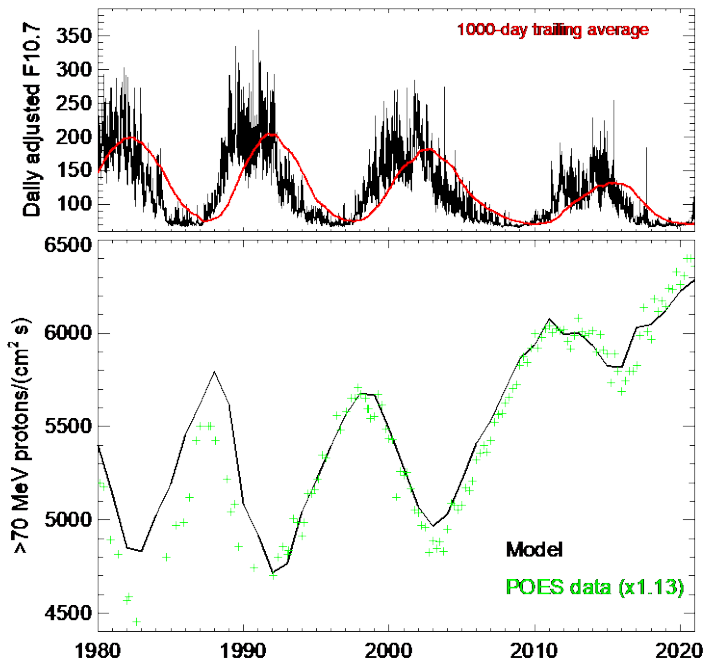
213
214
215
216
217
218

219 4 Model Comparison

220

221 To provide additional insight into the causes of observed variation in the SAA proton flux,
 222 theoretical predictions have been made with the proton radiation belt model of Selesnick et al.
 223 (2007), as updated by Selesnick and Albert (2019). Model results showing the maximum
 224 omnidirectional integral (>70 MeV) proton flux in the SAA region at POES altitude, as a
 225 function of time since 1980, are shown in Figure 5, for comparison to the observations in Figure
 226 1. The trend of generally increasing proton flux, with a superimposed solar-cycle modulation, as
 227 seen in the POES data, is also evident in the model results, except prior to about 1992 when a
 228 general increase is not predicted by the model.

229



230

231 **Figure 5.** (Top) Daily adjusted F10.7 (black) and 1000-day trailing average of F10.7 (red);
 232 (Bottom) Model results for omnidirectional >70 MeV proton flux in the SAA at POES altitude at
 233 $L=1.3$ (black). POES flux was multiplied by a factor of 1.13 (green) for ease of comparison with
 234 the model.

235

236 At the low (~ 800 km) POES altitude, the model proton flux results mainly from a balance
 237 between the CRAND source and energy loss caused by atmospheric drag. The balance is
 238 established, at this altitude, after a model run of a few decades and no initial condition is
 239 therefore required. The rate of energy loss depends on upper atmospheric density, including
 240 neutral gas and plasma density, that increases with solar EUV input, as parameterized in the
 241 model by solar F10.7. Therefore, the trend of increasing SAA flux is a direct result, in the model,
 242 of the decreasing F10.7 values during successive recent solar maxima, as shown in Figure 1. The
 243 phase lag from F10.7 maxima to proton flux minima, of ~ 500 days in both the model and
 244 observations, results from the average time scale of proton energy loss at this altitude.

245

246 The model also predicts that the maximum SAA proton flux is near $L=1.3$ for > 70 MeV protons,
 247 as observed. However, this result is somewhat dependent on other model inputs, such as values

248 of the radial diffusion coefficient and an additional, unspecified loss process, with a mean
 249 lifetime of 22 years, that was added to the model by Selesnick and Albert (2019) to match
 250 observed radiation belt flux values. These factors have only a minor influence on model results
 251 near L=1.3, but do change the results at higher L and therefore influence the location of the flux
 252 maximum.

253
 254 Similar model flux values (black line) across the first two solar cycles in Figure 5 result from
 255 similar corresponding F10.7 values. It is therefore unclear why the measured proton flux (green)
 256 showed generally increasing levels during this early period as well. A discrepancy between
 257 F10.7 and solar EUV flux during this period is possible or some other uncertainty in the model.
 258 However, generally similar time dependencies and absolute flux values in the data and model
 259 add confidence to the data interpretation over the forty year time scale shown.

260

261 **5 Discussion and Conclusions**

262

263 In general terms, the basic equation which balances thermal kinetic energy causing the
 264 atmosphere to expand against gravity pulling it earthward is (see Russell et al., 2016):

265

$$266 \quad n = n_0 \exp(-h/H)$$

267

268 where h is altitude and $H = kT/mg$ is the scale length over which thermal pressure decays
 269 exponentially at a given fixed temperature T. This equation of hydrostatic equilibrium states that
 270 the scale height is longer therefore the atmosphere decays more slowly with h when T is greater.
 271 This explains the basic physics of why the loss rate of inner zone protons is lower when there is
 272 less solar energy input to the atmosphere. The lag time between solar minimum as measured by
 273 F10.7 and peak proton flux corresponds to the thermal inertia of the atmosphere. Selesnick et al.
 274 (2007) used the NRLMSISE-00 atmosphere model to calculate trapped proton flux in an IGRF
 275 magnetic field model. Their Figure 11 shows the altitude profile for two sample neutrals (H and
 276 N₂) at different F10.7. When F10.7 increases from 60 to 220, the dominant N₂ concentration
 277 increases at each altitude. This is due to increased EUV heating of the atmosphere for which
 278 F10.7 serves as a proxy. When F10.7 is not as high on average, as was the case for the recent
 279 solar maximum compared with prior maxima shown in **Figure 1**, there will be less N₂ at a given
 280 altitude affecting collisional energy loss of protons. Figure 12 in Selesnick et al. (2007) shows
 281 that H⁺, He⁺ and O⁺ density decreases at a given altitude as F10.7 decreases. The inner zone
 282 protons lose energy primarily via Coulomb collisions with both free and bound electrons
 283 (Selesnick et al., 2007; Selesnick and Albert, 2019), explaining the higher flux levels above a
 284 fixed energy following weaker solar maxima.

285

286 The Solar Cycle 24 flux minimum (December, 2015), averaged over the three energy channels
 287 studied, was calculated to be 19% higher than the Solar Cycle 23 minimum (October, 2002) (**Fig.**
 288 **3**). The weaker Solar Cycle 24 solar maximum caused less atmospheric and ionospheric heating,
 289 thereby reducing inner zone proton energy loss via collisions and flux for the > 70 MeV energy
 290 channel shown in **Figures 1** and **2**. We found a similar trend in the >35 MeV and >140 MeV
 291 energy channels (**Fig. 3**). The flux increased from a high flux minimum in 2016 compared to
 292 prior minima since 1980 shown in **Figure 1**, to its highest maximum for the time period 1980 -
 293 2021 examined by June 2021 .

294
295 While the short term variation within a solar cycle leading to higher flux lagging solar minimum
296 is explained by the F10.7 variation within a solar cycle (Qin et al., 2014; Li et al., 2020; Lin et
297 al., 2020), the longer term trend for >70 MeV protons seen in **Figure 1**, also evident but not
298 noted by Qin et al. who examined NOAA POES flux at > 70 MeV from 1980 – 2010, requires
299 consideration of longer term solar variations, notably the Gleissberg cycle (Gleissberg, 1965;
300 Svalgaard et al., 2005; Feynman & Ruzmaikin, 2011, Pulkinen et al., 2001). Feynman &
301 Ruzmaikin (2011) described the Centennial Gleissberg Cycle as an approximately century-long
302 sinusoidal variation in the intensity of solar maximum and found evidence to suggest that Solar
303 Cycles 23 and 24 represent the minimum of this 80 to 100-year cycle. The onset of this
304 Gleissberg cycle minimum in solar activity indicates that the increasing proton flux discussed in
305 this paper is to be expected and serves to explain these results.

306
307 Note that Lin et al., (2020) recalibrated POES and MetOp satellite data using POES NOAA-15
308 as the reference standard but did not find a long-term increase in >16 MeV proton flux at
309 constant L = 1.2. We focused on the three higher energy channels of POES energetic proton
310 measurements: >35 MeV, >70 MeV and >140 MeV where electron contamination issues are
311 known to be less significant (Janet Green, private communication). It was found that both the
312 peak flux in the SAA and the flux at constant L=1.3 show the same long term trend. Further
313 comparison with measurements from other spacecraft such as Van Allen Probes (Li et al., 2020)
314 is warranted, including standardization of integral flux measurements across the POES data set
315 when compared with measurements from the Relativistic Electron Proton Telescope on Van
316 Allen Probes (Baker et al., 2013). However, the great value of the POES data set going back to
317 1980 is the unique long baseline used in the present study to identify the flux increase correlation
318 with reduced solar activity over four solar cycles. From a space weather hazard standpoint, this
319 long term increase in the flux of inner zone protons should be included in updated models of the
320 space radiation environment.

321

322 **Acknowledgments**

323 This study is supported by AFOSR grant FA9550-20-1-0339. E.B. acknowledges support from
324 the High Altitude Observatory Visitor Program, NCAR. We thank Drs. Janet Green, Rob
325 Redmon, and Juan Rodriguez for discussion of the POES data.

326

327 **Data Availability Statement**

328

329 F10.7 data come from the OMNI database: <https://omniweb.gsfc.nasa.gov/form/dx1.html>. The
330 data for POES are available at <https://satdat.ngdc.noaa.gov/sem/poes/data/>.

331

332 **References**

333 Baker, D. N., et al. (2013), The Relativistic Electron-Proton Telescope (REPT) Instrument on
334 Board the Radiation Belt Storm Probes (RBSP) Spacecraft: Characterization of Earth's Radiation
335 Belt High-Energy Particle Populations, *Space Sci. Rev.*, 179, 337– 381, doi:[10.1007/s11214-012-](https://doi.org/10.1007/s11214-012-9950-9)
336 [9950-9](https://doi.org/10.1007/s11214-012-9950-9)

337

- 338 Cook, W. R., Cummings, A. C., Cummings, J. R., Garrard, T. L., Kecman, B., Mewaldt, R. A.,
339 Selesnick, R. S., Stone, E. C., Baker, D. N., von Rosenvinge, T. T., Blake, J. B., & Callis, L. B.
340 (1993). PET: A proton/electron telescope for studies of magnetospheric, solar, and galactic
341 particles. *IEEE Transactions on Geoscience and Remote Sensing*, 31(3), 565– 571.
342 <https://doi.org/10.1109/36.225523>
343
- 344 Dragt, A. J. (1971), Solar cycle modulation of the radiation belt proton flux, *J. Geophys. Res.*,
345 76(10), 2313–2344.
- 346 Dyer, C. (2002), Radiation effects on spacecraft and aircraft, in Proceedings of the Second Solar
347 Cycle and Space Weather Euroconference, edited by H. Sawaya-Lacoste, Eur. Space Agency
348 Spec. Publ., ESA SP-477, 505 -- 512.
- 349 Evans, D.S., and M.S. Greer (2006), Polar orbiting environmental satellite space environment
350 monitor-2: Instrument descriptions and archive data documentation, *NOAA Technical*
351 *Memorandum, Boulder, Colorado OAR SEC 93, 93, version 2.0, 2006*,
352 https://satdat.ngdc.noaa.gov/sem/poes/docs/sem2_docs/2006/SEM2v2.0.pdf.
- 353 Feynman, J., & Ruzmaikin, A. (2011). The sun's strange behavior: Maunder minimum or
354 Gleissberg cycle? *Solar Physics*, 272(2), 351–363. <https://doi.org/10.1007/s11207-011-9828-0>
- 355 Ginet, Gregory & O'Brien, T. & Huston, S. & Johnston, W. & Guild, Timothy & Friedel, R. &
356 Lindstrom, C. & Roth, Christopher & Whelan, P. & Quinn, R. & Madden, D. & Morley, Steven
357 & Su, Yi-Jiun (2013). AE9, AP9 and SPM: New Models for Specifying the Trapped Energetic
358 Particle and Space Plasma Environment. *Space Science Reviews*. 179. 10.1007/s11214-013-
359 9964y.
- 360 Gleissberg, W. (1965), The eighty-year solar cycle in auroral frequency numbers. *J. Br. Astron.*
361 *Assoc.* 75, 227 – 231.
- 362 Gombosi T., [Physics of the Space Environment](https://doi.org/10.1017/CBO9780511529474) (1998), Cambridge University Press, Cambridge,
363 UK, [doi:10.1017/CBO9780511529474](https://doi.org/10.1017/CBO9780511529474)
- 364 Huston, S., G. Kuck, and K. Pfizter (1998), Solar cycle variation of the low-altitude trapped
365 proton flux, *Adv. Space Res.*, 21(12), 1625–1634.
- 366 Kuznetsov, N. V., N. I. Nikolaeva, and M. I. Panasyuk (2010), Variation of the trapped proton
367 flux in the inner radiation belt of the Earth as a function of solar activity, *Cosmic Res.*, 48(1), 80–
368 85.
369
- 370 Li, X., Xiang, Z., Zhang, K., Khoo, L., Zhao, H., Baker, D. N., & Temerin, M. A. (2020). New
371 insights from long-term measurements of inner belt protons (10s of MeV) by SAMPEX, POES,
372 Van Allen probes, and simulation results. *Journal of Geophysical Research: Space Physics*,
373 125(8). <https://doi.org/10.1029/2020JA028198>
374
- 375 Lin, R., Zhang, J., Zhang, X., Ni, B., Liu, S., Shi, L., et al. (2020). Long-term variations of >16-
376 MeV proton fluxes: Measurements from NOAA POES and EUMETSAT MetOp satellites.

- 377 *Journal of Geophysical Research: Space Physics*, 125, e2019JA027635.
378 <https://doi.org/10.1029/2019JA027635>
379
- 380 Nakano, G., and H. Heckman (1968), Evidence for solar-cycle changes in the inner-belt protons,
381 *Phys. Rev. Lett.*, 20(15), 806–809.
382
- 383 Pavón-Carrasco, F. J., & De Santis, A. (2016). The South Atlantic Anomaly: The key for a
384 possible geomagnetic reversal. *Frontiers in Earth Science*, 4, 40.
385
- 386 Pulkkinen, TI, H Nevanlinna, PJ Pulkkinen, M Lockwood (2001), [The Sun–Earth connection in
387 time scales from years to decades and centuries](https://doi.org/10.1023/A:1005299314802), *Space Science Reviews* 95 (1), 625–637,
388 <https://doi.org/10.1023/A:1005299314802>.
389
- 390 Qin, M., Zhang, X., Ni, B., Song, H., Zou, H., & Sun, Y. (2014). Solar cycle variations of
391 trapped proton flux in the inner radiation belt. *Journal of Geophysical Research: Space Physics*,
392 119(12), 9658–9669. <https://doi.org/10.1002/2014JA020300>
393
- 394 Rabin, V. J., D. S. Evans, H. H. Sauer, S. R. Sahn and M. Huynh (1995), TIROS/NOAA
395 Satellite Space Environment Data Archive Documentation: 1995 Update, *NOAA Technical*
396 *Memorandum, ERL SEL -86, Boulder, Colorado*,
397 [https://satdat.ngdc.noaa.gov/sem/poes/docs/sem1_docs/TIROS-](https://satdat.ngdc.noaa.gov/sem/poes/docs/sem1_docs/TIROS-NOAA_SEM_Data_Archive_Documentation_1995-update.pdf)
398 [NOAA_SEM_Data_Archive_Documentation_1995-update.pdf](https://satdat.ngdc.noaa.gov/sem/poes/docs/sem1_docs/TIROS-NOAA_SEM_Data_Archive_Documentation_1995-update.pdf)
399
- 400 Reames, D., Ng, C., & Tylka, A. (1999). Energy-dependent ionization states of shock-
401 accelerated particles in the solar corona. *Geophysical Research Letters*, 26, 3585–3588.
402 <https://doi.org/10.1029/1999GL003656>
403
- 404 Russell, C. T., J. G. Luhmann, R. J. Strangeway (2016), *Space Physics: An Introduction*,
405 Cambridge University Press, ISBN1107098823, 9781107098824
406
- 407 Selesnick, R. S., & Albert, J. M. (2019). Variability of the proton radiation belt. *Journal of*
408 *Geophysical Research: Space Physics*, 124(7), 5516–5527.
409 <https://doi.org/10.1029/2019JA026754>
410
- 411 Selesnick, R. S., D. N. Baker, A. N. Jaynes, X. Li, S. G. Kanekal, M. K. Hudson, and B. T. Kress
412 (2014), Observations of the inner radiation belt: CRAND and trapped solar protons, *J. Geophys.*
413 *Res. Space Physics*, 119, 6541–6552, doi:10.1002/2014JA020188.
414
- 415 Selesnick, R. S., Looper, M. D., & Mewaldt, R. A. (2007). A theoretical model of the inner
416 proton radiation belt. *Space Weather*, 5(4), n/a-n/a. <https://doi.org/10.1029/2006SW000275>
417
- 418 Selesnick, R. S., Hudson, M. K., & Kress, B. T. (2010). Injection and loss of inner radiation belt
419 protons during solar proton events and magnetic storms. *Journal of Geophysical Research:*
420 *Space Physics*, 115(A8), n/a-n/a. <https://doi.org/10.1029/2010JA015247>
421
- 422 Singer, S. F. (1958), Trapped albedo theory of the radiation belt, *Phys. Rev. Lett.*, 1, 181-- 183.

- 423
424 Stassinopoulos, E. G., & Raymond, J. P. (1988). The space radiation environment for electronics.
425 *Proceedings of the IEEE*, 76(11), 1423–1442. <https://doi.org/10.1109/5.90113>
426
- 427 Svalgaard, L., Cliver, E.W. and Kamide, Y. (2005), Sunspot cycle 24: Smallest cycle in 100
428 years? *Geophys. Res. Lett.*, 32, L01104, doi:[10.1029/2004GL021664](https://doi.org/10.1029/2004GL021664)
429
- 430 Thébault, E. et al. (2015), International Geomagnetic Reference Field: the 12th generation. *Earth*
431 *Planets Space* 67,79. doi:10.1186/s40623-015-0228-9
432
- 433 Van Allen, J. A., Ludwig, G. H., Ray, E. C., & McIlwain, C. E. (1958). Observation of high
434 intensity radiation by satellites 1958 Alpha and Gamma. *Journal of Jet Propulsion*, 28, 588–
435 592. Van Allen, J. A., Ludwig, G. H., Ray, E. C., & McIlwain, C. E. (1958).
436
- 437 Yermolaev, Y. I., Lodkina, I. G., Khokhlachev, A. A., Yermolaev, M. Yu., Riazantseva, M. O.,
438 Rakhmanova, L. S., Borodkova, N. L., Sapunova, O. V., & Moskaleva, A. V. (2021). Drop of
439 solar wind at the end of the 20th century. *Journal of Geophysical Research: Space Physics*,
440 126(9). <https://doi.org/10.1029/2021JA029618>